

NEW ALGORITHMS FOR THE ANALYSIS OF WASTE CHARACTERIZATION

Xiaoqin J. Guo, Richard. C. Hagenauer
ORTEC/AMETEK
801 S. Illinois Ave.
Oak Ridge, TN 37830

ABSTRACT

Nondestructive assay of gamma-ray emitting nuclear waste requires modeling because it is not practical to prepare a standard that matches the physical and nuclear properties of every waste item. The use of a high-purity germanium (HPGe) detector simplifies the spectral analysis process. Many models use simplified efficiency determinations and attenuation corrections. These models often work well for medium-sized items measured at detector-to-item distances that are at least half of the largest dimension of the object. Other models use a hybrid Monte Carlo approach, but the detector efficiency parameters must be established at an additional cost.

A new algorithm has been developed to reduce these complications and limitations while retaining acceptable accuracy. This algorithm uses a simple mixed-nuclide gamma calibration, the detector crystal diameter and length, crystal type (n-type or p-type), thickness of the germanium dead layer, and distance from the top of the end cap to the germanium active layer to compute the detector intrinsic efficiency. The intrinsic efficiency for the front and side of the detector are correlated with the detector diameter and length. Corrections for the gamma rays from the item being measured are calculated voxel by voxel. These new algorithms have been implemented in the ORTEC® ISOTOPIC software version 4. Results show significant improvement for items counted as close as 10 cm, and are useful for the measurement of items positioned in a low-level drum counter.

INTRODUCTION

When the detector is positioned close to a large item containing radioactivity a significant amount of activity enters the HPGe detector from the side. The classic far-field correction¹ for matrix attenuation does not account for this because it assumes all gamma-rays enter the detector normal to the front surface. An algorithm has been developed that utilizes the crystal diameter and length to automatically estimate the efficiency of the detector from the side surface as well as the front surface. Only one point-source calibration, positioned normal to the front surface of the detector crystal, is needed. This point source, whose activity is traceable to a national standard, must contain gamma rays that span the energy range of the gamma rays emitted by the nuclides present in the measured item.

CHARACTERIZING THE DETECTOR INTRINSIC EFFICIENCY

The algorithms take advantage of detector characterization. Initially, full-energy peak intrinsic efficiency² is needed for the detector used to make the analysis. To obtain that information a point-source calibration is needed at a fixed distance from the face of the detector.

$$\Omega = 2\pi \cdot \left(1 - \frac{d}{\sqrt{d^2 + R^2}}\right) \quad (1)$$

$$\varepsilon_p = \frac{n}{N} \quad (2)$$

where:

- S = subtended solid angle (radians)
- R = radius of the detector (cm)
- d = distance from the calibration point source to the detector (cm)
- \mathcal{G} = full energy peak efficiency of the detector at distance d
- n = number of gamma rays detected at the full energy peak from the source
- N = number of gamma rays emitted at the full energy peak from the source
- \mathcal{G}_f = full energy peak intrinsic efficiency

Note that in order to compute the intrinsic efficiency the diameter of the detector crystal is needed.

A working detector has a dead layer of germanium and an aluminum end cap to house the detector. Attenuation by the can and dead layer of germanium must be taken into account for realistic detector characterization. See Figure 1. Now, the intrinsic peak efficiency for a realistic detector can be determined as shown in Equation 5.

$$C_1 = e^{-\mu_e l_e} \quad (3)$$

$$C_2 = e^{-\mu_{al} l_{al}} \quad (4)$$

$$\varepsilon_{if} = \frac{\varepsilon_p \cdot 4\pi}{C_1 \cdot C_2 \cdot \Omega} \quad (5)$$

where:

- C_1 = attenuation correction factor for the aluminum end cap
- μ_e = linear attenuation coefficient for the aluminum end cap (cm^{-1})
- l_e = aluminum end cap thickness (cm)
- C_2 = attenuation correction factor for the dead layer of germanium
- μ_{dl} = linear attenuation coefficient for germanium (cm^{-1})
- l_{dl} = thickness of the germanium dead layer (cm)
- \mathcal{G}_f = full-energy peak intrinsic efficiency for the front of the detector

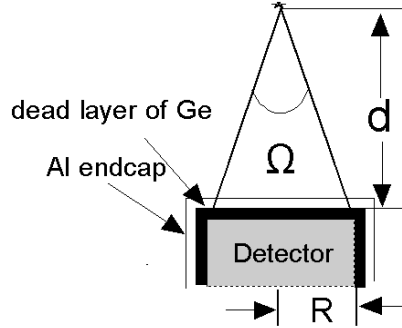


Figure 1. HPGe Detector with a Dead Layer of Germanium and Aluminum Endcap.

The side of the detector also detects gamma rays and must be included in the overall full peak intrinsic efficiency. To estimate the average length of gamma-ray cylinder penetration length, CPL , assume that, for side detection, the detector is a bar. See Figure 2. The average thickness of the penetration distance is computed using Equation 6, 7.

$$CPL = \sqrt{2} \cdot R \quad (6)$$

If you know the relative fraction of gamma-ray activity remaining in the crystal when penetrated from the side and from the front, you can determine the total peak area intrinsic efficiency for the side.

$$\mathcal{E}_{is} = \mathcal{E}_{if} \frac{(1 - e^{-\mu \cdot CPL})}{(1 - e^{-\mu \cdot l})} \quad (7)$$

where:

- \mathcal{G}_s = side full-energy peak intrinsic efficiency
- μ = linear attenuation coefficient for germanium at energy of the gamma ray penetrating the detector (cm^{-1})
- l = length of the detector (cm)

Thus, information about the length of the detector crystal is needed to compute the side efficiency.

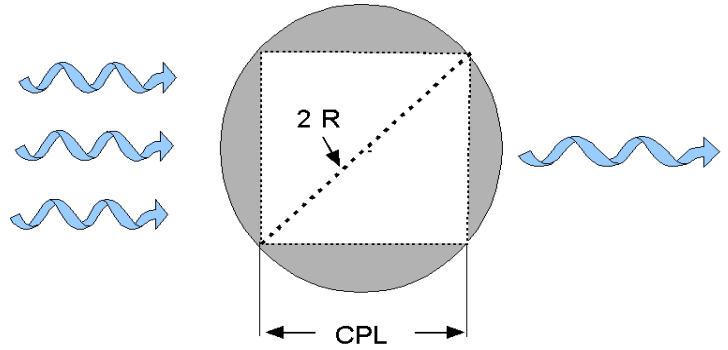


Figure 2 Top View of a Detector Used to Estimate the Average Penetration Distance.

COMPUTING ACTIVITY

For a point source with no significant attenuation, positioned with an offset greater than the diameter of the detector, both the side and top of the detector will see activity. To compute the activity of the source, both detector efficiencies are needed. See Figure 3.

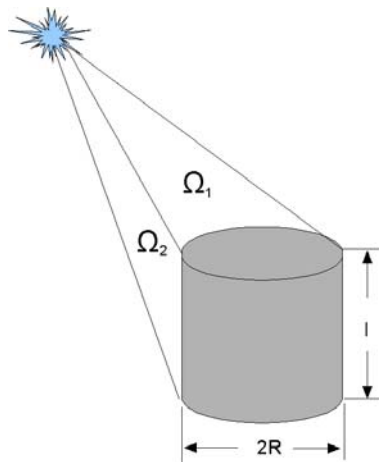


Figure 3. Activity of a Point Source Interacting with the Top and Side Surfaces of a Detector.

Once the efficiencies of both the front and side of the detector are determined, the activity of the point source can be computed as shown in Equation 8.

$$Act_{ps} = \frac{CR \cdot 4\pi}{\left(\epsilon_{if} \cdot C_1 \cdot C_2 \cdot \Omega_1 + \epsilon_{is} \cdot C_3 \cdot C_4 \cdot \Omega_2\right) \cdot k} \quad (8)$$

where:

- Act_{ps} = reported activity (Bq)
- S_1 = the solid angle subtended on the top surface of the detector (radians)
- S_2 = the solid angle subtended on the side surface of the detector (radians)
- C_3 = attenuation through the side of the end cap and cup holding the detector
- C_4 = attenuation through the side dead layer of Ge
- k = constant involving the yield (branching ratio), decay corrections, and unit conversion factors ((emitted/Bq)

When computing the activity of a item, the volume must be subdivided into small voxels, each of which must be corrected for matrix and container corrections. The activity of a voxel, Act_i , is shown in Equation 9.

$$Act_i = \frac{CR \cdot V_i \cdot 4\pi}{\left(\epsilon_{if} \cdot C_1 \cdot C_2 \cdot \Omega_1 + \epsilon_{is} \cdot C_3 \cdot C_4 \cdot \Omega_2\right) \cdot V \cdot k} \quad (9)$$

Note that for a box, the volume of each voxel is the same. However, for a cylinder or other items, the voxel volumes might not be the same and the activity must be weighted accordingly.

$$Act_{item} = \frac{1}{\sum_{i=1}^n \frac{D_{1i} \cdot D_{2i} \cdot D_{3i}}{Act_i}} \quad (10)$$

where:

- Act_{item} = activity of item being measured (Bq)
- V = volume of the item (cm²)
- V_i = volume of the i^{th} voxel(cm²)
- D_{1i} = matrix correction for the i^{th} voxel
- D_{2i} = inner container correction factor for the i^{th} voxel
- D_{3i} = outer container correction factor for the i^{th} voxel
- n = number of voxels

VALIDATING THE ALGORITHMS

Sources with known activity were used to validate the algorithms. First, sources were positioned at a standoff of 20 cm and measured at different offsets to validate the improvement using the side efficiency. See Figure 4. The results were plotted as shown in Figure 5.

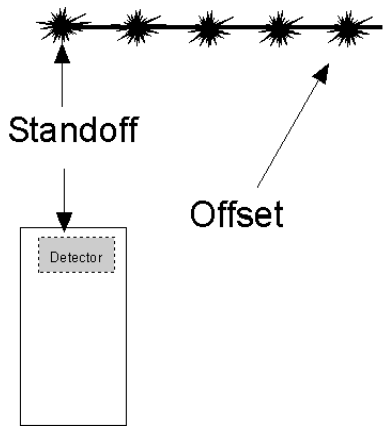


Figure 4. Different Source Positions Were Used to Validate the Algorithm.

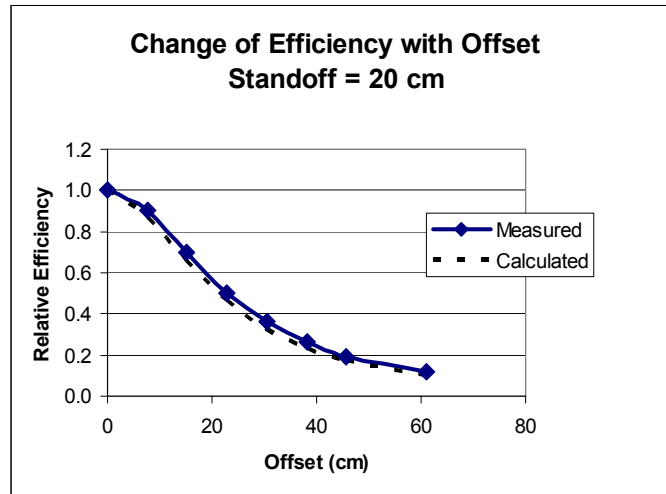


Figure 5. Results of Offset Measurements.

Data were collected from many detectors with varying crystal aspect ratios. These calculated measured results varied from measured by less than 10% in all measurements. The data shown in Figure 5 varied by less than 2%.

A 50 kg box of KCl was used to validate the algorithm for a homogenous box. Natural ^{40}K was used to provide the known activity. To establish the accuracy of close for closeup measurements a detector was positioned a various distances from the box and the results compared to the known ^{40}K content. Natural ^{40}K background was subtracted from all spectra. The standard far-field measurement analysis was compared to the analysis obtained from the close geometry algorithm. The results are shown in Figure 6.

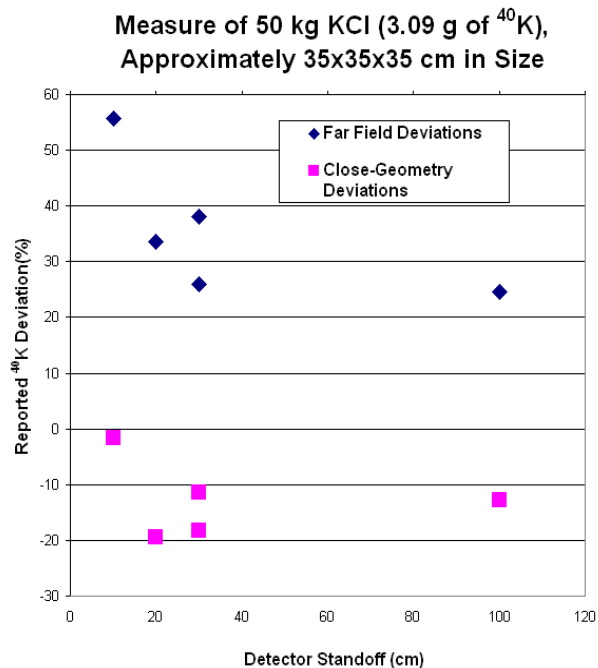


Figure 6 Comparison of the Close-Geometry Algorithm with the Far-Field Algorithm for the Measurement of ^{40}K .

These results show that analyzing ^{40}K spectra using the close-geometry algorithm gives results in good agreement with the accepted value of ^{40}K for standoff distances of 10 cm to 100 cm. As would be expected, the far-field method results are high because the extra activity entering the detector from the side is not accounted for in the calibration.

Typically, containers of nuclear waste are not as homogeneous as the ^{40}K content in a box of KCl. For very low level waste measurements, multiple detectors must be positioned very close to 208-liter drums for maximum sensitivity. These drums are frequently rotated to simulate a more homogeneous container as most models initially assume item homogeneity. To simulate a nuclear waste drum, a 208-liter drum was filled with very nonhomogeneous, medium-density matrix and spiked with ^{134}Cs , ^{137}Cs , and ^{60}Co . Three measurements were made at three drum locations, as shown in Figure 7, and averaged. The detector was positioned only 10 cm from the surface of the drum at all three locations. The drum was rotated, measured, and analyzed using the close-geometry algorithm and the far-field algorithm. A comparison of the two methods is shown in Table 1.

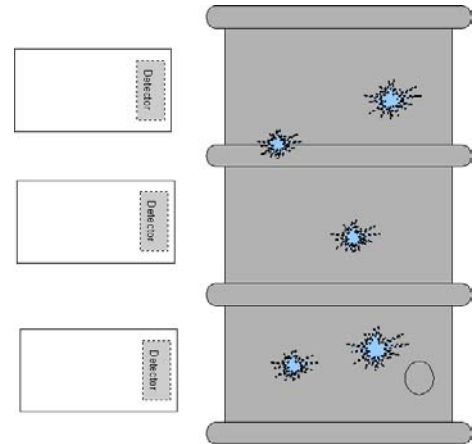


Figure 7. Using the Close-Geometry Algorithm to Measure Drums with Nonhomogeneous Matrices.

Table 1. Comparison of Close Geometry with Far-Field Geometry Correction Algorithm for a Nonhomogeneous Drum.

Nuclide	Far Field (Bq)	Close Geo. (Bq)	Accepted (Bq)	FF % Diff	CG %Diff
Cs-134	8399	5402	4978	69	8.5
Cs-137	14911	9805	9850	51	-0.5
Co-60	11803	7770	8178	44	-5.0

The close-geometry results are very close to the accepted activities. As expected, the far-field results are high because a large fraction of the activity enters the side of the detector and this activity is not accounted for in the calibration.

Future experiments are planned to established the best distance/sensitivity/accuracy correlation.

SUMMARY

The close-geometry algorithm show greatly improved accuracy for measurement of radioactive items when the detector is positioned close to the item being measured and no collimator is used. By using the detector crystal diameter and length in addition to other detector parameters, improved accuracy can be obtained without additional calibration effort. This algorithm has been incorporated into the new version of the ISOTOPIC software.

REFERENCES

1. D. Reilly, N. Ensslin, and H. Smith Jr., Passive Nondestructive Assay of Nuclear Material, United States Regulatory Commission, NUREG/CR 5550, 1991.
2. G. Gilbert, Practical Gamma-Ray Spectroscopy, John Wiley and Sons Ltd, West Sussex, England, 1995.